DOI: 10.1002/ppsc.201600175

Article type: Full Paper

Biodegradable Passion Fruit-Like Nano-Architectures as Carriers for Cisplatin Prodrug

*Domenico Cassano, Melissa Santi, Valentina Cappello, Stefano Luin, Giovanni Signore, and Valerio Voliani**

D.C., M.S., Dr. V.C., Dr. G.S., Dr. V.V.
Center for Nanotechnology Innovation @NEST, Istituto Italiano di Tecnologia, P.zza San Silvestro, 12 - 56127, Pisa (PI), Italy.
E-mail: valerio.voliani@iit.it
D.C., M.S., Dr. S.L.
NEST, Scuola Normale Superiore, P.zza San Silvestro, 12 - 56126, Pisa (PI), Italy
Dr. S.L.
NEST, Istituto Nanoscienze – CNR, P.zza San Silvestro, 12 - 56126, Pisa (PI), Italy

Keywords: biodegradation, cisplatin, human pancreatic carcinoma, hollow silica, gold nanoparticle

Accumulation of inorganic nanostructures in the excretory system organs increases their likelihood of toxicity and interference with common medical diagnoses. Thus, one of the major concerns regarding their clinical translation is related to their persistence in organisms. Here we demonstrate that nano-architectures composed by hollow silica nanocapsules embedding arrays of ultrasmall gold nanoparticles undergo biodegradation in cellular environment affording small, potentially clearable building blocks. Furthermore, we present their exploitation in glutathione-triggered release of covalently loaded cisplatin prodrug. This endogenously triggered release leads to high cytotoxicity to human pancreatic carcinoma cells, setting the way for promising applications to synergistic dual chemo/radio-therapy and radio-imaging.

1. Introduction

Co-therapy, an increasingly employed approach to the treatment of neoplasms, is exploited by the co-delivery of various drugs or the synergistic administration of a mix of therapies, such as chemo/radio-therapy.[1]

An elegant approach to achieve co-therapy is by employing multifunctional nanoparticles.[2] Moreover, the inclusion of active agents in multifunctional nanostructures usually increases the former efficacy in a number of ways, among which: i) improving their solubility and stability,[3] ii) increasing their specificity and local concentration eventually by controlled release [4–6] and iii) making possible synergistic action of multiple therapies.[7,8] Engineered metal nanoparticles can actually combine therapeutic properties, such as efficient drug delivery, hyperthermia or radiation-therapy enhancement,[9,10] with imaging functionalities, like photoacoustic or x-ray-based diagnostics.[11,12]

This allows for the development of theranostic tools designed for specific patients or diseases.[3,5,13]

In this context, noble metal nanoparticles are particularly appealing but their average size for *in vivo* applications is usually above 20 nm.[14] This size can lead to severe clearance issues, with accumulation in excretory organs.[3] Indeed, poor body clearance is one of the most relevant hurdles preventing their clinical translation.[14,15]

On the other hand, metal nanoparticles functionality is usually severely altered when their size is decreased down to few nanometers,[16] even if some of them still maintain optimal physiological properties.[15,17]

In order to combine the intriguing behavior of metal nanoparticles with the possibility of organism excretion,[18] we have recently introduced a passion fruit-like biodegradable nano-architecture composed by 90 nm hollow silica nanospheres embedding arrays of 3 nm gold nanoparticles in polymeric matrices.[19] In these nanocapsules the silica shell both protects the material in the inner cavity from the environment and provides an easily modifiable/functionalizable surface. Gold nanoparticles confer the physical behavior needed

for imaging/therapeutic applications,[10,20] while the cationic polymer is covalently functionalizable with active molecules, among which dyes, drugs and chelating agents.[19]

Here we demonstrate the biodegradation of the nanocapsules into potentially kidney-clearable building blocks in cellular environment by transmission electron and confocal microscopy and we report their application as endogenous-triggered cisplatin prodrug carriers toward human pancreatic carcinoma cells, resulting in a promising nano-architecture for synergistic dual chemo/radio-therapy.

2. Results and discussion

Figure 1A shows the complete synthetic approach for the production of the passion fruit-like nano-architectures containing an average of 4.9% w/w of gold on the total weight of freeze-dried samples. Nanocapsules were synthesized as reported elsewhere with slight modifications, demonstrating the versatility of the synthetic protocol.[19] In particular, poly(L-lysine) 15-30 kDa was covalently functionalized with AlexaFluor-488 on about 5% of the amines and used for the synthesis of nanocapsules (AuSiA). Gold nanoparticles showing a diameter of 2.8±0.4 nm (**Figure S1**) and coated by poly(sodium 4-styrene sulfonate) (PSS) were aggregated in spherical arrays by modified poly(L-lysine) (PL) by means of ionic interactions, and then the silica shell was grown on this template by a modified Stöber method resulting in 90 nm nano-architectures. The composition of the silica shell around gold arrays is related to the simultaneous presence of both amines from PL and aromatic moieties from PSS. Indeed, aromatic additives have been demonstrated to be required for the formation of a silica shell around PL templates in the synthesis of hollow silica microspheres.[21] The silica shell formation mechanism was investigated during the synthetic process by TEM observation every 15 minutes (**Figure S2**). After 15' from the beginning of the reaction TEOS was adsorbed and hydrolyzed in the gold-polymer arrays. Then, the silica shell began to be formed

until the complete formation of the capsule after 2h. It is interesting to notice that: i) the concentration of gold nanoparticles appears to decrease during the capsules formation, and ii) the silica shell of the final capsules does not show gold nanoparticles inclusion while they are present in the shell during its formation. These findings suggest that a fraction of gold nanoparticles are probably expelled during the process of consolidation of the shell.

After the nanocapsules production, their external surface was modified with (3-aminopropyl)triethoxysilane (APTES) and functionalized by AlexaFluor-647, without affecting their colloidal stability (AuSiAA). The success of the reaction was demonstrated by optical and DLS measurements. Optical behavior in PBS buffer of AuSiAA, AuSiA (nanocapsules with AlexaFluor-488 in the cavity and without surface functionalization), and AuSi (basic nanocapsules without dyes) are reported in **Figure 1B**. The UV-vis spectrum of AuSiAA shows a typical scattering pattern including the absorption bands of both AlexaFluor-488 and -647, while the plasmon band of gold nanoparticles is almost completely hidden. UV-vis spectra of AuSiA and AuSi show, respectively, the absorption band of AlexaFluor-488 and the extinction band of gold nanoparticles. The fluorescence spectra of AuSiAA were collected by irradiating at 488 nm and 647 nm and the emission bands from the dyes were recorded, confirming the presence of both fluorophores in the nano-architecture. It is interesting to notice that AlexaFluor-488 can suffer fluorescence quenching and Raman enhancement effects caused by the vicinity of the dyes to gold nanoparticles surface in the polymeric arrays.[4,19,22] The presence of a negligible second emission band at 670 nm by exciting at 488 nm can be related to a cross-excitation effect of AlexaFluor-647. The zeta-potential of the nano-architectures (**Figure S3**) varies from -26 mV for the as-synthesized nanostructures to +21 mV after the surface modification with APTES. After the covalent modification with AlexaFluor-647, a negatively charged dye (**Figure 1A**), the zeta-potential decreases to +6 mV, confirming the success of the functionalization.

The degradation of the nanocapsules to silicic acid, polymers, and ultrasmall gold nanoparticles (metal core diameter: 2.8±0.4 nm, hydrodynamic diameter: 3.22±0.39 nm, **Figure S4**) was demonstrated in human serum in about 24 hours.[19] Thus, we performed confocal and TEM biodegradation experiments on cultured cells in a similar timeframe. AuSiAA were incubated with MIA PaCa-2 cells for 30 minutes. Then, confocal images were collected by laser excitation on both dyes in AuSiAA at 0h, 24h and 48h after incubation. The uptake of AuSiAA was confirmed and the calculated Pearson's coefficient at t=0 was 0.967±0.001 (**Figure 2A**), indicating a high degree of colocalization between the fluorescence signals.[23,24] As expected, internalized nanocapsules observed by TEM demonstrate an undamaged structure immediately after cellular uptake (**Figure 2B**, 0h column). The recorded images (Figure 2B and **Figure S5**) point out that AuSiAA are mainly internalized by macropinocytosis or clathrin-independent endocytosis and entrapped in endocytic vesicles in populations of 1-15 nanoparticles/vesicle.[25] This is consistent with the confocal images, in which colocalized fluorescent spots of various sizes are observable in cells. The colocalization of the fluorescence signals decreased (**Figure 2A**) through 48h, showing a final Pearson's coefficients of 0.682±0.005. It is important to remember that red spots are related to AlexaFluor-647, the dye linked to the surface of the silica shell, while the green spots are related to AlexaFluor-488, covalently linked to poly(L-lysine). Notably, during the 48h, fluorescence signal in the green channel arises from wider and more dispersed zones than the spots recorded at t=0h, while the one in the red channel, when present, it is still confined in spots similar to the ones at t=0h that colocalize with the green channel. This behavior could suggest that the erosion of the nano-architectures begins from their outside, and that the AlexaFluor-647/APTES conjugates are probably able to escape from vesicles and from the cells. These hypothesis are supported by TEM characterizations. Indeed, after 24h (**Figure 2B**, 24h column) the endocytic vesicles show: i) nano-architectures that are partially eroded from the surface, ii) agglomerates of gold nanoparticles on a matrix, and iii) free gold

nanoparticles. It is interesting to notice that, during the degradation process, the silica shell shows a swollen and less defined structure. This seems to confirm that the erosion mechanism is likely related to an externally started hydrolysis of the silica shell.[26] After 48h very few undamaged nanocapsules are detectable, while some vesicles contain some ropy structures (Figure 2B, 48h column), which can be associated to a possible re-condensation of the silicic acid.[19]. Moreover, the ultrastructure analysis of cells confirms that there was no cytotoxic effect due to the treatment with AuSiAA (**Figure S6**). It is worth to notice that ultrasmall gold nanoparticles could be coated by endogenous thiols, such as GSH, after biodegradation of nanocapsules.[6] The effect of the coating exchange was tested by incubation of gold nanoparticles in 5 mM GSH solution (**Figure S4**).[6] Remarkably it was observed that their hydrodynamic diameter slightly increases to 3.81±0.45 nm, suggesting that they do not undergo aggregation when coated by GSH, thus enhancing the possibility of their renal clearance.[15]

The biodegradation of the nano-architectures to potentially kidney-clearable building blocks makes them promising tools for therapy/diagnosis of neoplasms. Thus, we included in their cavity a prodrug, in order to produce an endogenous-triggered releasing agent suitable for dual chemo/radio-therapy. Indeed, while prodrugs show a chemotherapeutic activity, gold nanoparticles can be used for enhancing of x-ray radiation therapy or x-ray imaging.[10,12]

Cis-diamminedichloroplatinum(II) (cisplatin) and its analogues are among the most commonly used chemotherapeutics for a number of neoplasms owing to their ability to inhibit the growth of cancer cells by interfering with DNA-transcription. Their action mechanism involves the establishment of 1,2-intrastrand crosslinks, in a process referred to as DNA-platination.[7,27,28] However, their efficacy is limited by associated severe systemic toxicities, such as nephrotoxicity, neurotoxicity, ototoxicity, and emetogenesis.[27]

Pt(IV) prodrugs are hidden forms of cisplatin, whose production can be triggered by endogenous thiols, which lead to reductive elimination of axial ligands.[27,29] In this context,

Pt(IV) complexes provide an attractive alternative to Pt(II) compounds because their inertness results in fewer side effects, decreased drug inactivation and longer half-life in the bloodstream.[7,30] The inclusion of this prodrug in the biodegradable nanostructures can enhance its specificity and efficiency together with the possibility to combine synergistic action of different therapies.

Cisplatin prodrug c,t,c-[$PtCl_2(NH_3)_2(OH)(O_2CCH_2CH_2CO_2H)$], was synthesized and characterized as reported.[7,31] The prodrug was then covalently linked to poly(L-lysine) and the AuSiP system composed (**Figure 3A**). It is worth to notice that AuSiP shows a negative-charged surface because it was not coated by APTES. This was due to no further surface modification requirements at this stage, such as conjugation to targeting moieties, resulting in a possible decreased internalization with respect to AuSiAA.[25] The amount of metal atoms in AuSiP was quantified by ICP-MS in 4.9% and 1.4% w/w of, respectively, gold and platinum on the total freeze-dried sample weight. The efficacy of AuSiP was tested on MIA PaCa-2 cells for 72h (**Figure 3B**), using the nanocapsules without the prodrug (AuSi) as control sample. The resulting dose/response profile can be correlated to the biodegradation of AuSiP followed by the endogenous-triggered release and vesicles escape of cisplatin. Indeed, there are no relevant cytotoxic effects during the first 24 hours, in agreement with the biodegradation timeframe. After the biodegradation of AuSiP, the prodrug can interact with intracellular free thiols, such as glutathione (GSH).[6] GSH reduces Pt(IV) to Pt(II) causing the release of the two axial ligands and leading to *in situ* production of cisplatin.[8] Interestingly, we observed more than 80% of cellular death in 72h at an AuSiP concentration of 2 μg/mL, corresponding to 0.14 μM of prodrug. This demonstrates the possible application of these nano-architectures as biodegradable carriers and their interesting effect over human pancreatic carcinoma cells.[32]

3. Conclusion

In summary we demonstrated the biodegradation of passion fruit-like nano-architectures in cellular environment by both confocal and transmission electron microscopy. Moreover we evidenced the versatility of these nanostructures by the functionalization on both their internal cavity and external surface. Finally, we employed them as carriers for endogenous-triggered cisplatin release on human pancreatic carcinoma cells. Such nano-architectures are promising agents that could help to fill the gap between inorganic nanomaterials and oncology. *In vivo* experiments on the clearance of nanocapsules by the renal pathway are ongoing, together with their application in radiotherapy and diagnostics. Synergistic integration of biodegradable passion fruit-like nano-architectures with biomimetic strategies and active targeting moieties can lead to the development of next generation nanotools.

4. Experimental Section

Materials: AlexaFluor-488 and -647 were purchased from Invitrogen. All the other chemicals were purchased from Sigma-Aldrich. Every reactive was used as it was without further purification.

Synthesis of c,t,c-[$PtCl_2(OH)_2(NH_3)_2$]: The method used was based on the one previously described by Hall et al.[31] 0.40 g of cis-[$PtCl_2(NH_3)_2$] (1.33 mmol) were suspended in 10 mL milliQ water and 14 mL of H_2O_2 30% w/v (10-fold excess) were added. The mixture was stirred for 1 h at 50 ˚ C. Then it was cooled to 0 ˚ C and 10 mL of a saturated water solution of NaCl were added. The resulted pale yellow powder was collected by filtration and washed with cold water, ethanol and diethyl ether, and dried in a vacuum pump, yielding 223 mg of c,t,c-[$PtCl_2(OH)_2(NH_3)_2$] (0.67 mmol, 50%).

Synthesis of c,t,c-[$PtCl_2(NH_3)_2(OH)(O_2CCH_2CH_2CO_2H)$]: The method used was based on that previously described by Dhar et al.[7] To a solution of c,t,c-[$PtCl_2(OH)_2(NH_3)_2$] (0.2 g, 0.6 mmol) in anhydrous DMSO (16 mL) was added succinic anhydride (0.06 g, 0.6 mmol) and

the reaction mixture was stirred at room temperature for 12h. The solution was freeze-dried and 10 mL acetone were added to precipitate a light yellow solid, which was collected by filtration and washed several times with acetone, diethyl ether, and then dried in a vacuum pump, yielding 0.16 g of c,t,c-[$PtCl_2(NH_3)_2(OH)(O_2CCH_2CH_2CO_2H)$] (0.37 mmol, 62%). ^1H NMR (DMSO-d_6) 6.18-5.66 (m, 6H), 2.44-2.33 (m, 4H). ^{13}C NMR (DMSO-d_6) 31.16; 31.74; 174.55; 180.17.

Synthesis of drug-modified poly(L-lysine) – PLp.: 0.5 mg of c,t,c-[$PtCl_2(NH_3)_2(OH)(O_2CCH_2CH_2CO_2H)$] were dissolved in 400 µL of PBS buffer and mixed with 40 µL of freshly made 0.21 M EDC/NHS solution (3.6 mg/2.2 mg in 100 µL cold milliQ water, EDC: N-(3-dimethylaminopropyl)-N'-ethylcarbodiimide hydrochloride, NHS: N-Hydroxysuccinimide). After 10' stirring at room temperature, 75 µL of 20 mg/mL MilliQ solution of poly(L-lysine) hydrobromide 15-30 kDa (1.5 mg) were added to the reaction mixture and the resulting solution was stirred overnight at room temperature. The modified poly(L-lysine) was collected and washed three times with PBS buffer by Amicon 10K filter units, and then dissolved in 800 µL PBS buffer.

Synthesis of dye-modified poly(L-lysine) – PLa: 1.5 mg of poly(L-lysine) hydrobromide 15-30 kDa were dissolved in 780 µL of PBS and 200 µg of AlexaFluor488-NHS ester (10 mg/mL, DMSO solution) were added to the solution. The reaction mixture was kept under stirring overnight at RT, and it was used without further purification.

Synthesis of gold nanoparticles: Gold seeds with a diameter of approximately 3 nm were prepared according to the following procedure. To 20 mL of milliQ water were added 10 µL of poly(sodium 4-styrene sulfonate) (30% aqueous solution) and 200 µL of $HAuCl_4$ aqueous solution (10 mg/mL). During vigorously stirring, 200 µL of sodium borohydride (4 mg/mL in milliQ water) were added quickly, and the mixture was stirred vigorously for other 2 minutes. After the addition of $NaBH_4$, the solution underwent some color changes until becoming

brilliant orange. Before its use the solution was generally aged for at least 30 minutes and employed without further purification.

Synthesis of gold nanoparticles arrays: 1 mL of gold nanoparticles solution was added to a 2 mL plastic vial followed by 40 µL of the PBS solution of PLa or PLp, and the mixture was allowed to stir for 30 minutes at room temperature. The as synthesized gold aggregates were collected by centrifugation (13400 rpm for 3 minutes), suspended in 100 µL of milliQ water and sonicated for maximum 4 minutes.

Synthesis of AuSiA and AuSiP: In a 100 mL round bottomed flask were added 70 mL of absolute ethanol followed by 2.4 mL of ammonium hydroxide solution (30% in water), and 40 µL of tetraethyl orthosilicate (TEOS, 98%). The solution was allowed to stir for 20` at RT. 2 mL of the gold nanoparticles arrays previously prepared were added to the reaction flask and the solution was allowed to stir for further 3h. The as-synthesized AuSi nanoparticles (AuSiA or AuSiP from, respectively, PLa and PLp arrays) were collected by 30 minutes centrifugation at 4000 rpm, washed twice with ethanol to remove unreacted precursors and suspended in 1 mL of ethanol. A short spin centrifugation was employed in order to separate the structure over 150 nm from the supernatant, which was recovered as a pink- iridescent solution. The solution was centrifuged at 13400 rpm for 5 minutes, suspended in 500 µL milliQ water, sonicated for 5 minutes and freeze-dried overnight. Usually, about 1.5 mg of a brilliant pink powder is obtained, which remains stable for at least 1 year if stored sealed in the dark at 10 ˚C.

Surface coating and functionalization of AuSiA The method used was based on the one previously described.[33] 150 µg of AuSiA were dissolved in 10 mL of anhydrous ethanol and 100 µL of APTES were added to the solution. After 15 minutes mixing at 55°C the reaction solution was centrifuged 3 times (2 minutes each at 13400 rpm) in ethanol and the precipitate recovered in 200 µL of anhydrous DMF. Then, 2.5 µL of AlexaFluor647-NHS ester (10 mg/mL, DMSO solution) were added to the mixture and the solution was mixed at RT for at

least 3 hours. The colloid (AuSiAA) was centrifuged 3 times (2 minutes each at 13400 rpm) in PBS and recovered in 100 μL of the final solvent (TEA, PBS, serum etc.).

UV/Vis spectrophotometry: Extinction spectra were collected by means of a double beam spectrophotometer Jasco V-550 UV/VIS equipped with quartz cuvettes of 1.5 mm path length and normalized to the maximum absorbance. PBS (1X) buffer was employed as solvent.

Fluorescence spectrometry: Fluorescence spectra were collected by means of a Cary Eclipse fluorimeter equipped with quartz cuvettes of 1.5 mm path length. Excitation and emission slits of 10 nm were employed and a photomultiplier voltage between 500 V and 700 V, depending on the concentration of the sample. All the samples were dispersed in PBS (1X) buffer before collecting the spectra.

DLS measurements: Measurements were performed in standard capillary cells DTS 1060 (for z-potential measurements) or 50 μL standard cuvette (for size measurements) on a Malvern Zetasizer nano ZS90, following the manufacturer instructions. Colloids with concentration between 1 and 10 μg/mL were analyzed in PBS buffer at pH 7.4. Each value reported is the average of five consecutive measurements.

Cell Culture: Human pancreatic carcinoma cells (MIA PaCa-2) were purchased from the American Type Culture Collection (ATCC). This cell line was growth using a previously reported protocol.[34]

Confocal microscopy: Cells were seeded 24 h before the experiments into glass-bottom Petri dish (WillCo-dish GWSt-3522) to reach 80-90% of confluence. Incubation of maximum 30 μg of nanoparticles was performed for 30 minutes at 37 °C, 5% CO_2 in DMEM with 10% FBS in a total volume of 500 μL. After incubation cells were washed twice with PBS, fresh medium was added and the samples were analyzed by confocal microscopy. Cells were imaged using a Leica TCS SP5 SMD inverted confocal microscope (Leica Microsystems AG) interfaced with Ar and HeNe laser for excitation at 488 nm and 647 nm respectively. Cells were mounted in a thermostat chamber at 37°C (Leica Microsystems) and viewed with a 40x

1.5 NA oil immersion objective (Leica Microsystems). The pinhole aperture was set to 1.0 Airy. All images were analyzed using ImageJ software 1.48v and colocalization was evaluated using JACoP plugin.

Viability tests: Cytotoxicity was evaluated by using a tetrazolium salt, 2-(2-methoxy-4-nitrophenyl)-3-(4-nitrophenyl)-5-(2,4-disulfophenyl)-2*H* tetrazolium, monosodium salt (WST-8) assay. MIA PaCa-2 cells ($1x10^4$ cells per well) were seeded in 96-well plates. After culture for 24 hours, the cells were incubated with a 2% serum-containing medium in the presence of nanoparticles at nanoparticle concentration ranging from 0 to 50 µg/mL for 30 minutes at 37 °C. After the incubation, the medium was removed and cells were washed twice with PBS and kept in fresh DMEM. For each experimental time point cells were incubated with WST-8 reagent (10 µL) and 2% serum-containing medium (90 µL) for 2 hours. Absorbance (at 450 nm) was measured using a microplate reader (Glomax Discovery, Promega). The percentage of cell viability was determined by comparing drug-treated cells with the untreated cells (100% viability). Data represent the average of three independent experiments. Error bars are SD from three independent experiments.

Electron microscopy: TEM observations of nanoparticles: measures were carried out on a ZEISS Libra 120 TEM operating at an accelerating voltage of 120 kV, equipped with an in-column omega filter. The colloidal solutions were deposited on 300-mesh carbon-coated copper grids. TEM observation on cells: MIA PaCa-2 cells were grown to confluence in 35-mm dishes and incubated with maximum 30 µg of AuSiAA for 30 minutes at 37 °C. Different times of resting after treatment were tested (0h, 24h, 48h).

After the resting period, MIA PaCa-2 cells monolayers were fixed for 1h at RT in a 1.5% glutaraldehyde solution in sodium cacodylate buffer. Cells were scraped, collected and centrifuged at 13200 rpm at RT for 15 minutes in the same fixative solution until a visible pellet was obtained. Then, cells were kept in a new fixative solution overnight at 4 °C. Cells were then rinsed and embedded with a conventional embedding procedure. Briefly, the

samples were post-fixed with osmium tetroxide (2% OsO_4 in sodium cacodylate buffer; 0.1 M pH 7.4), rinsed, stained and blocked with 3% solution of uranyl acetate in 20% ethanol. Finally, they were dehydrated, embedded in epoxy resin (Epon 812, Electron Microscopy Science, Hatfield, PA, USA), and baked for 48 h at 60 °C. In order to perform ultrastructural analysis, 90 nm sections of treated samples were cut by using a UC7 (Leica Microsystems, Vienna, Austria) and stained with uranyl acetate - lead citrate.

ICP-MS Analysis: Nanoparticles were dissolved in 200 μL aqua regia (prepared with ICP-MS grade HCl and HNO_3) and digested under microwave irradiation (200 °C/7 minutes) in Teflon-lined vessels. The resulting solution was diluted to 2 mL with ICP-MS grade water, and content of Si, Pt and Au was determined by ICP-MS analysis against a standard calibration curve.

Supporting Information Supporting Information is available from the Wiley Online Library or from the author.

Acknowledgements
We thank Dr. Mauro Gemmi and Prof. Fabio Beltram for their support. The manuscript was written through contributions of all authors. All authors have given approval to the final version of the manuscript. Domenico Cassano and Melissa Santi contributed equally to this work.

Received: ((will be filled in by the editorial staff))
Revised: ((will be filled in by the editorial staff))
Published online: ((will be filled in by the editorial staff))

[1] E. Lim, T. Kim, S. Paik, S. Haam, Y. Huh, K. Lee, *Chem. Rev.* **2015**, *115*, 327.
[2] K. K. Ng, G. Zheng, *Chem. Rev.* **2015**, *115*, 11012.
[3] T. Sun, Y. S. Zhang, B. Pang, D. C. Hyun, M. Yang, Y. Xia, *Angew. Chemie Int. Ed.* **2014**, *53*, 12320.
[4] L. Bergamini, V. Voliani, V. Cappello, R. Nifosì, S. Corni, *Nanoscale* **2015**, *7*, 13345.
[5] V. Voliani, G. Signore, O. Vittorio, P. Faraci, S. Luin, J. Peréz-, J. Peréz-Prieto, F. Beltram, *J. Mater. Chem. B* **2013**, *1*, 4225.
[6] C. S. Kim, B. Duncan, B. Creran, V. M. Rotello, *Nano Today* **2013**, *8*, 439.
[7] S. Dhar, W. L. Daniel, D. a. Giljohann, C. a. Mirkin, S. J. Lippard, *J. Am. Chem. Soc.* **2009**, *131*, 14652.

[8] J. Li, Z. Lyv, Y. Li, H. Liu, J. Wang, W. Zhan, H. Chen, H. Chen, X. Li, *Biomaterials* **2015**, *51*, 12.
[9] J. F. Hainfeld, F. A. Dilmanian, D. N. Slatkin, H. M. Smilowitz, *J. Pharm. Pharmacol.* **2008**, *60*, 977.
[10] Y.-S. Yang, R. P. Carney, F. Stellacci, D. J. Irvine, *ACS Nano* **2014**, *8*, 8992.
[11] L. E. Cole, R. D. Ross, J. M. Tilley, T. Vargo-Gogola, R. K. Roeder, *Nanomedicine* **2015**, *10*, 321.
[12] H. Lusic, M. W. Grinstaff, *Chem. Rev.* **2013**, *113*, 1641.
[13] E. C. Dreaden, A. M. Alkilany, X. Huang, C. J. Murphy, M. A. El-Sayed, *Chem. Soc. Rev.* **2012**, *41*, 2740.
[14] M. L. Etheridge, S. A. Campbell, A. G. Erdman, C. L. Haynes, S. M. Wolf, J. McCullough, *Nanomedicine Nanotechnology, Biol. Med.* **2013**, *9*, 1.
[15] M. Yu, J. Zheng, *ACS Nano* **2015**, 150714141008001.
[16] L.-Y. Chen, C.-W. Wang, Z. Yuan, H. Chang, *Anal. Chem.* **2015**, *87*, 216.
[17] K. Zarschler, L. Rocks, N. Licciardello, L. Boselli, E. Polo, K. P. Garcia, L. De Cola, H. Stephan, K. A. Dawson, *Nanomedicine Nanotechnology, Biol. Med.* **2016**, *12*, 1663.
[18] R. Kumar, I. Roy, T. Ohulchanskky, L. Vathy, *ACS Nano* **2010**, *4*, 699.
[19] D. Cassano, D. Rota Martir, G. Signore, V. Piazza, V. Voliani, *Chem. Commun.* **2015**, *51*, 9939.
[20] D. Kim, S. Park, J. H. Lee, Y. Y. Jeong, S. Jon, *J. Am. Chem. Soc.* **2007**, *129*, 7661.
[21] K. Van Bommel, J. Jung, S. Shinkai, *Adv. Mater.* **2001**, *13*, 1472.
[22] E. Dulkeith, A. C. Morteani, T. Niedereichholz, T. A. Klar, J. Feldmann, S. A. Levi, F. C. J. M. van Veggel, D. N. Reinhoudt, M. Möller, D. I. Gittins, *Phys. Rev. Lett.* **2002**, *89*, 203002.
[23] J. Adler, I. Parmryd, *Cytom. Part A* **2010**, *77*, 733.
[24] V. Voliani, F. Ricci, S. Luin, F. Beltram, *J. Mater. Chem.* **2012**, *22*, 14487.
[25] Y. Jiang, S. Huo, T. Mizuhara, R. Das, Y.-W. Lee, S. Hou, D. F. Moyano, B. Duncan, X.-J. Liang, V. M. Rotello, *ACS Nano* **2015**, *9*, 9986.
[26] H. Gao, O. A. Goriacheva, N. V. Tarakina, G. B. Sukhorukov, *ACS Appl. Mater. Interfaces* **2016**, *8*, 9651.
[27] X. Wang, Z. Guo, *Chem. Soc. Rev.* **2013**, *42*, 202.
[28] Z. H. Siddik, *Oncogene* **2003**, *22*, 7265.
[29] S. Dhar, F. X. Gu, R. Langer, O. C. Farokhzad, S. J. Lippard, *Proc. Natl. Acad. Sci. U. S. A.* **2008**, *105*, 17356.
[30] H. Xiao, R. Qi, S. Liu, X. Hu, T. Duan, Y. Zheng, Y. Huang, X. Jing, *Biomaterials* **2011**, *32*, 7732.
[31] M. D. Hall, C. T. Dillon, M. Zhang, P. Beale, Z. Cai, B. Lai, A. P. J. Stampfl, T. W. Hambley, *J. Biol. Inorg. Chem.* **2003**, *8*, 726.
[32] U. Olszewski, F. Ach, E. Ulsperger, G. Baumgartner, R. Zeillinger, P. Bednarski, G. Hamilton, *Met. Based. Drugs* **2009**, *Iv*, 1.
[33] X. Ling, D. Reinhoudt, J. Huskens, *Langmuir* **2006**, 8777.
[34] D. Porciani, G. Signore, L. Marchetti, P. Mereghetti, R. Nifosì, F. Beltram, *Mol. Ther. Acids* **2014**, *3*, e144.

Captions

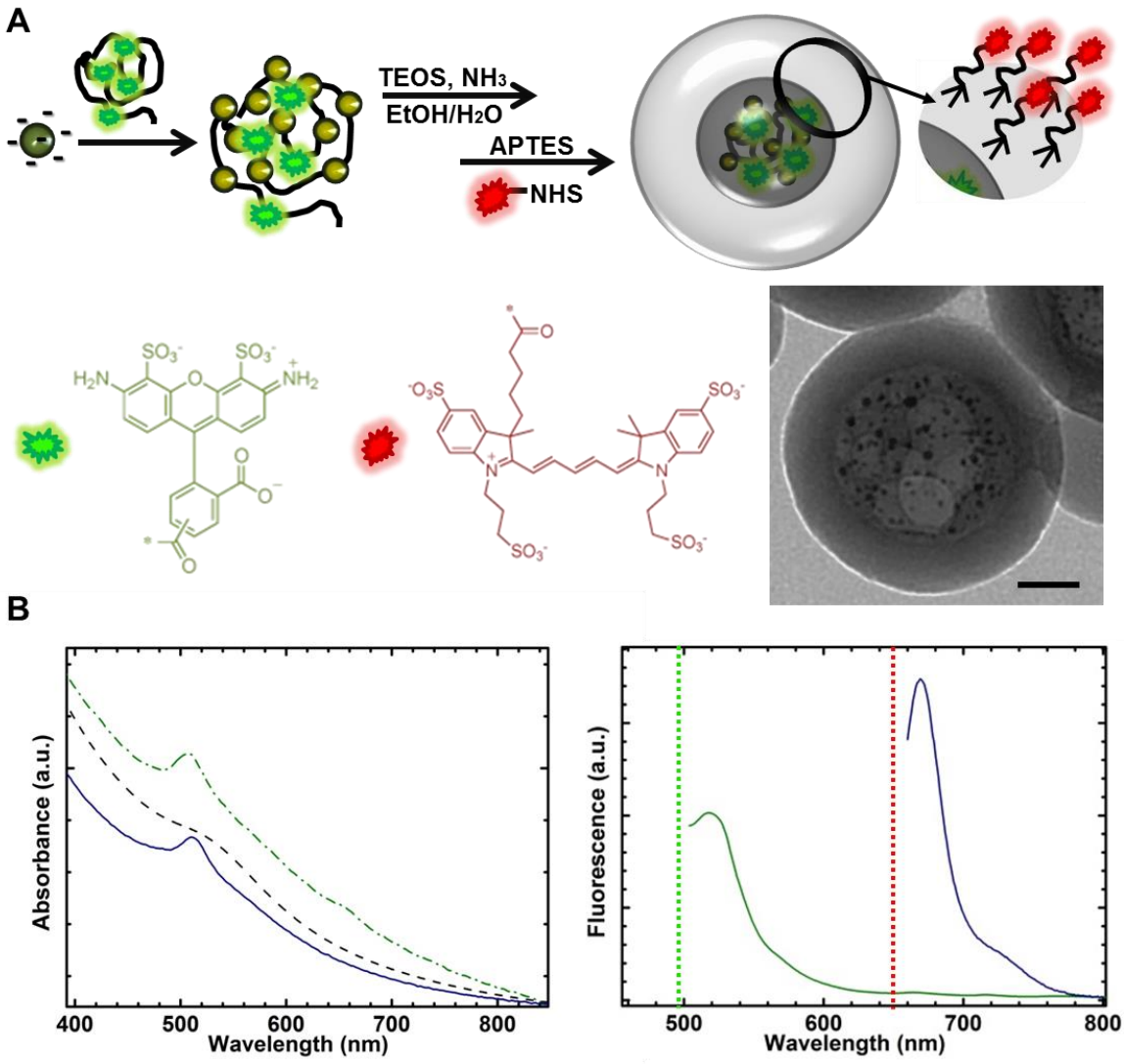

Figure 1. A) Scheme of the synthesis of AuSiAA and structure of the dyes. AlexaFluor-488 was covalently linked to around 5% of the amines of poly(L-lysine) before the formation of the polymer arrays with 2.8±0.4 nm gold nanoparticles. The surface of the nanocapsule was modified by APTES and functionalized by AlexaFluor-647. Bottom-right: typical TEM image of the passion fruit-like nano-architectures, Scalebar: 25 nm. B) Left panel: UV-visible spectra in PBS buffer of AuSi (dashed black), AuSiA (continuous blue line) and AuSiAA (green dash-dotted line). Right panel: AuSiAA fluorescence spectra in PBS buffer. Exc. 488 nm, dotted green, and 647 nm, dotted red, for, respectively, green and blue emission lines.

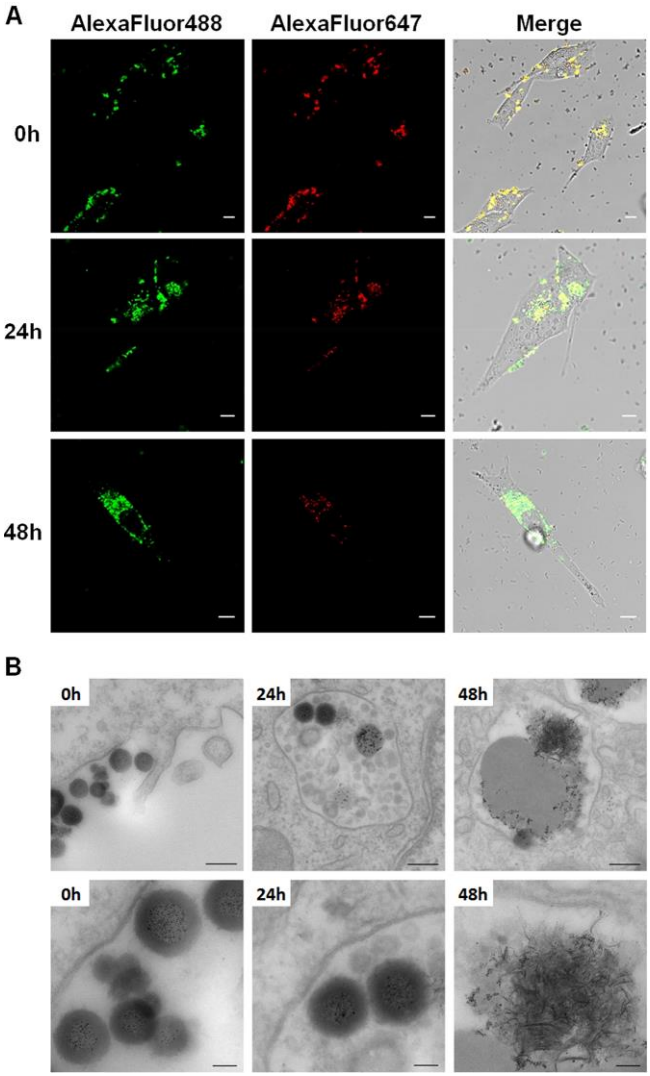

Figure 2. A) Representative confocal assay showing the decrease in fluorescence colocalization as a function of time after internalization of AuSiAA in MIA PaCa-2 cells. Cells were incubated 30 minutes with AuSiAA before starting the observations (t=0h). Green and red LUTs describe AlexaFluor-488 and AlexaFluor-647 respectively (exc. 488 nm, em. 500-550 nm; and exc. 633 nm, em. 650-700 nm). Pearson's coefficients decreased from 0.967±0.001 at t=0h to 0.682±0.005 at t=48h. Scalebar: 10 µm. B) TEM analysis of internalization, storage and degradation of AuSiAA in MIA PaCa-2 cells during 48h. The images show the internalization of AuSiAA (left, t=0 after cellular uptake), their storage and degradation in the endosomal compartment (center, t=24h) and the complete biodegraded nano-architectures (right, t=48h). Bottom panels are magnifications of the top ones. Scalebars: 200 nm top panels, 50 nm bottom ones.

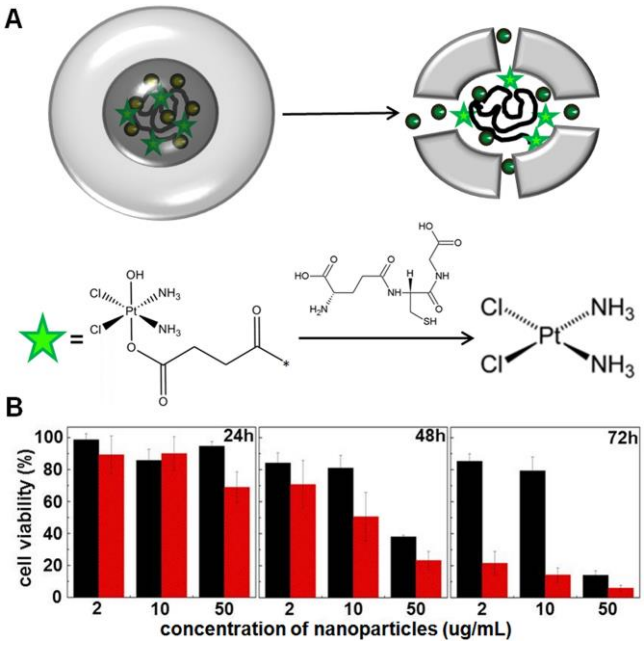

Figure 3. A) Top: scheme of a AuSiP nanostructure and its degradation. Bottom: structure of the Pt(IV) prodrug complex and the endogenous-triggered release of cisplatin by reduction of the metal ion due to the presence of thiols, such as glutathione (GSH), in cellular environment. B) Cell viability experiments on MIA PaCa-2 cells. Concentrations are expressed in μg of freeze-dried nanoparticles/mL of solution, and related to AuSiP (red) and AuSi (black).

Text for TOC

Biodegradation in cellular environment of passion fruit-like nano-architectures is demonstrated together with their exploitation in glutathione-triggered release of cisplatin toward human pancreatic carcinoma cells.